End-current injection contacts for anisotropic materials: Fabrication and application to the quasi-one-dimensional conductor $NbSe_3$

A. F. Isakovic,[1,2,*] K. Cicak,[1,†] and R. E. Thorne[1]
[1]*Laboratory for Atomic and Solid State Physics, Cornell University, Ithaca, New York 14853, USA*
[2]*National Synchrotron Light Source, Brookhaven National Laboratory, Upton, New York 11973, USA*
(Received 19 October 2007; revised manuscript received 15 January 2008; published 28 March 2008)

We have developed a technique for making low-resistance end-current injection contacts to geometrically, electronically, and mechanically anisotropic crystals of charge-density-wave (CDW) conductors. Transport measurements on $NbSe_3$ show that contact resistances are reduced by nearly 2 orders of magnitude compared with the standard side-contact geometry, and yield qualitatively similar results for the contact-sensitive phase-slip process. This end-contact technique should be useful for characterizing collective transport in fully gapped CDW conductors such as TaS_3, for studying CDW physics on scales smaller than 10 μm, and more broadly for characterizing other materials with large electronic and mechanical anisotropies.

DOI: 10.1103/PhysRevB.77.115141 PACS number(s): 71.45.Lr, 72.10.−d, 73.40.Ns, 81.65.Cf

Electrical transport measurements on bulk conducting materials typically employ one of a handful of contact configurations. Metal probes can be patterned on a substrate, and then the sample placed on top; probes may be pushed into the sample's top surface; or probes may be lithographically patterned on the top surface. However, for many highly anisotropic materials, these contact methods are inadequate. In quasi-one-dimensional (1D) conductors such as $NbSe_3$, TaS_3, and $K_{0.3}MoO_3$, the ratio of the longitudinal to transverse single-particle conductance is typically $\sim 10^2-10^3$,[1,2] reflecting large differences between interchain and intrachain hoppings and tunneling.[2,3] Contacts applied to the side of these elongated and often whiskerlike crystals inject current along the low-conductance direction, leading to large contact resistances, large local Ohmic heating, and inhomogeneous current and electric field profiles in the vicinity of the contact.[4] In charge-density-wave (CDW) conductors such as $K_{0.3}MoO_3$ and *o*-TaS_3 where the Peierls transition fully gaps the Fermi surface, CDW depinning, and motion, which dramatically increase the longitudinal conductance, can increase the conductance anisotropy to 10^6 or more at helium temperatures.[2]

The inhomogeneities in field and current densities associated with side contacts [Fig. 1(a)] occur on a longitudinal scale of roughly the crystal thickness times the square root of the conductance anisotropy, or 5–50 μm for typical samples.[4] As a result, side contacts are poorly suited to probing CDW physics at length scales of 10 μm and below. They can produce shear and phase slip in the CDW condensate, smearing out the depinning transition and the spectral width of the coherent oscillations that accompany CDW motion, and generating large-amplitude low-frequency electrical noise.

Side-current injection has proved particularly limiting in transport studies on fully gapped CDW materials such as *o*-TaS_3. One example is the study of the phase-slip process by which CDW current is converted to single-particle current near current contacts. Phase slip involves addition or removal of CDW wave fronts via formation and motion of dislocations in the CDW superlattice.[5–8,12,13] It is driven by gradients in the CDW phase corresponding to strains in the CDW superlattice[7,8,11,14,15] produced in response to an excess voltage V_{PS},[6,9,10] the phase-slip voltage. Like a spring in a gravitational field, the CDW compresses near one contact (where wave fronts are removed) and stretches near the other (where they are added).[11,14,15] The local phase-slip rate is a highly nonlinear function of strain, and so is largest near the current contacts. The integral of the local phase-slip rate gives the local CDW current density and velocity, which grow from zero near the contacts to their bulk values between them.[11]

In partially gapped $NbSe_3$, the phase-slip voltage V_{PS} measured using side-current injection contacts is independent of current contact separation for separations larger than 10 μm,[6,9,10] but at smaller separations (comparable to the scale of the effects of anisotropic current injection) a puzzling decrease in V_{PS} has been reported.[16] Spatially resolved voltage measurements on $NbSe_3$ (Ref. 11) have yielded CDW current and strain profiles that are qualitatively consistent with those obtained from spatially resolved x-ray[14] and optical[15] measurements and with theory.[11,13] However, similar transport measurements on more anisotropic and fully gapped TaS_3 have yielded results that cannot be readily interpreted.[17]

The obvious solution to these problems is to form current contacts to faces that are perpendicular to the highly conducting axis of the sample, as shown in Fig. 1(b). Unfortunately, because the bonding is much stronger along the one-

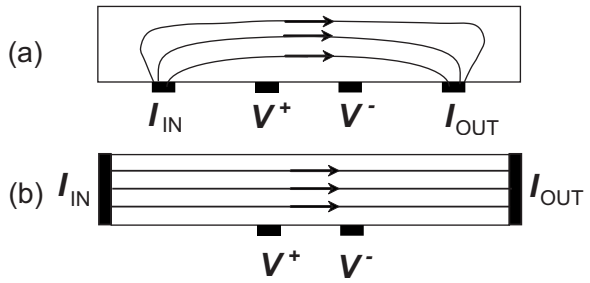

FIG. 1. Schematic illustration of the electric field lines within a sample when current is injected through (a) side contacts and (b) end contacts.

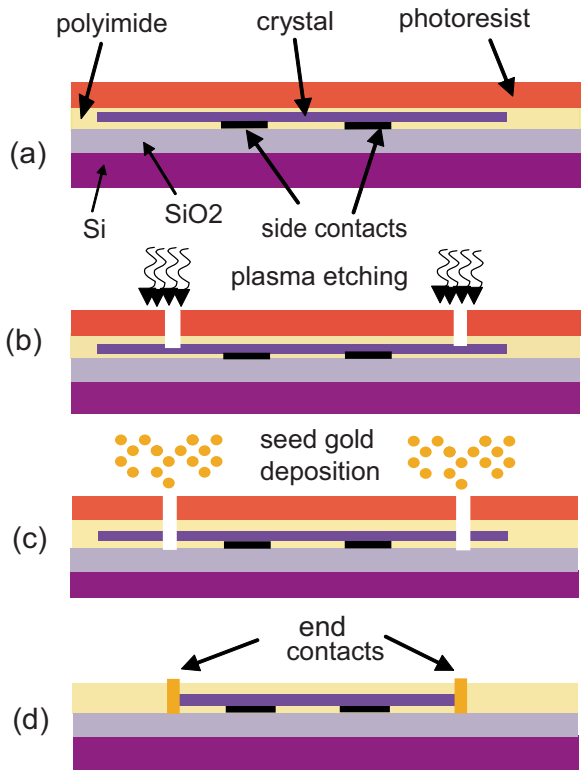

FIG. 2. (Color online) Fabrication of end contacts. (a) A crystal is held to gold side contacts and a SiO_2 covered Si wafer by a spin-coating layer of polyimide. A layer of photoresist is then spun onto the polyimide. (b) The photoresist is patterned and developed to expose the polyimide at the desired positions of the end contacts. The polyimide and $NbSe_3$ are removed through these windows by successive reactive ion etching steps. (c) A gold seed layer is deposited by e-beam evaporation. (d) The completed sample, after electroplating of additional gold onto the seed layer.

dimensional molecular chains than perpendicular to them, $NbSe_3$, TaS_3, and related materials cannot be cleaved to expose planes normal to the chains. When cut, they shred into multiple filaments. Even if they could be cleaved, the cross-sectional area of typical crystals is only $1-10\ \mu m^2$ compared with lengths of millimeters, so forming purely "end" contacts that did not wrap around the sides of the crystal would still be difficult.

Here, we describe a method for microfabricating end-current injection contacts to anisotropic materials. These contacts are mechanically robust and can survive multiple thermal cycles under moderate cooling and/or heating rates of 10–20 K/min. They provide dramatically reduced contact resistances to the moderately anisotropic CDW conductor $NbSe_3$. We use this method to re-examine the phase-slip process in $NbSe_3$, measuring the CDW current (I_C) as a function of the phase-slip voltage (V_{PS}). The qualitative results reported with side contacts are reproduced, but with some quantitative differences. Our experiments and process development focused on $NbSe_3$, because we have extensive data on its transport properties collected using conventional contact configurations and because we and others have previously developed methods for reliably side-contacting these samples and microfabricating structures using them. The real benefit of the end contact method, however, will be in study of more anisotropic and fully gapped materials such as TaS_3, where extreme anisotropy, extremely large low-temperature resistivities, and a more chemically reactive surface have made contact problems especially severe.

TABLE I. Typical reactive ion etch parameters used to etch polyimide and $NbSe_3$, for applied materials RIE system.

Parameter	Polyimide	$NbSe_3$
Gas	O_2	CF_4
Chamber pressure	30 mTorr	30 mTorr
Gas flow	20 SCCM	30 SCCM
Etch rate	38 nm/min	18 nm/min

The basic steps in our process are illustrated in Fig. 2. A single-crystal $NbSe_3$ sample with typical dimensions of a few millimeters long by 6–15 μm wide by 0.4–1.2 μm thick is placed on a SiO_2 covered Si substrate with predeposited 2 μm wide and 100 nm thick gold voltage probes. These probes have little perturbative effect on the current and field profiles within the sample.[3,10,11,18] The sample is held in close contact with the substrate by spinning a layer of polyimide PI285 of thickness 190–360 nm, produced by slowly and steadily increasing the spin speed from 1000 to 4500 rpm over 30–60 s. A layer of photoresist (Shipley 1811 or 1818) is spun to a thickness of 1.2–2.0 μm on top of the polyimide, and is then baked, patterned, exposed through a mask, developed to expose polyimide at the desired current contact positions, and finally postbaked.

Reactive ion etching (RIE) is then used in two stages (Fig. 2). First, an oxygen plasma removes the polyimide above the current contact positions. Then a carbon hexafluoride (CF_4) plasma removes the $NbSe_3$ to form a gap in the crystal. Table I gives typical gas flows, chamber pressures, and etch rates.

Extensive trials using angled evaporation proved unsuccessful in producing reliable, mechanically robust metal end-current contacts, so an alternative method was developed. E-beam evaporation is used to deposit a 150 Å titanium adhesion layer followed by a 1200 Å gold (Au) seed layer. A thick final layer of gold—650–900 nm, comparable to the $NbSe_3$ sample's thickness—is deposited by electroplating onto the seed layer using a standard gold plating solution bath. The deposition rate was 70 nm/min and approximately linear in time for constant bath temperature and the chosen bath current. Table II gives the parameters of the electroplating process. Typical RIE undercuts did not exceed 3°–5°, allowing reasonably uniform deposition of the gold seed layer and full coverage of the etched end of the crystal dur-

TABLE II. Typical parameters used to electroplate gold in forming the end contacts.

Parameter	Value
Bath temperature	60 °C
Bath current	20 mA
Range of plating rates	56–83 nm/min

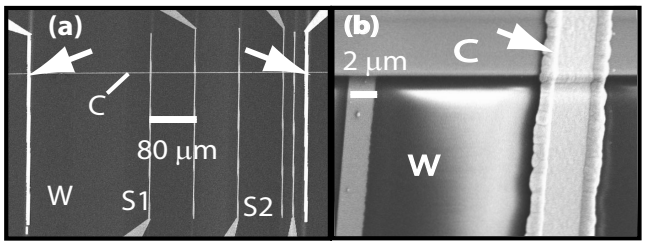

FIG. 3. (a) SEM image of a complete sample, showing the crystal (C), substrate (W), five side contacts (S1 and S2 and those used in measurements in Fig. 4), and two end contacts (indicated by arrows). (b) A close-up image of an end contact (indicated by an arrow) and one side contact.

ing electroplating. Additional details of the fabrication process development are available in Ref. 18.

Figure 3(a) shows a scanning electron microscopy (SEM) image of a completed structure comprised of a $NbSe_3$ crystal, side voltage contacts, and end-current contacts. Figure 3(b) shows a close-up of an end-current contact and a voltage contact. The region of overgrown gold visible in Fig. 3(b) can be removed,[19] but is insulated from the crystal by polyimide and photoresist and so does not affect electrical measurements.

Our present success rate in fabricating end contacts of the quality shown in Fig. 3 is about 40%. This is mainly limited by the large sample-to-sample variation in thickness and cross-sectional shape. The sample thickness affects the CF_4 etch time and electrodeposition time needed to form the current contacts, and the cross-sectional shape affects the quality of the contact between the sample and the voltage probes patterned on the substrate. Some process variability also results because the sample disturbs the flows of polyimide and photoresist during spinning, producing some thickness nonuniformity near the sample.

The final samples studied had end-current contacts separated by 500 μm and five side voltage contacts with separations of 20 or 80 μm. Data for two $NbSe_3$ samples will be presented. Sample A is 1.3 μm thick and 9 μm wide, while sample B is 0.9 μm thick and 6 μm wide. Both samples were free of visible longitudinal thickness steps, associated with small angle grain boundaries, and so etched uniformly. SEM images as in Fig. 3(b) show that the electroplated current contacts fill the entire etched volume. Cross-sectional SEM imaging of the $NbSe_3$-metal junction was not possible because of the crystal's tendency to shred into fibers rather than to cleave. Transport measurements were performed in a helium closed cycle refrigerator as described elsewhere.[10]

The end-current contacts described above provide much lower contact resistances to $NbSe_3$ than conventional side contacts. For $NbSe_3$ crystals of the cross-sectional dimensions studied here, side contacts give contact resistances at room temperature of 100–300 Ω,[10,11] depending upon the state of oxidation of the crystal's surface. End contacts give contact resistances of 3–6 Ω, nearly 2 orders of magnitude smaller, and dropping to 0.4 Ω at T=45 K.

Apart from the issue of the directionality of the electric field lines, evaporated contacts have also been useful in decreasing the contact resistance toward few ohm range.[20] Depinning fields E_T and the sharpness of the onset of CDW motion at E_T are at least comparable to those obtained with side contacts. When the CDW depins, large-amplitude $1/f$-like noise is generated due to inhomogeneous CDW current flow and CDW shear. End contacts give lower noise levels than side contacts. These results indicate that the end contacts provide uniform and longitudinal current injection and that the interface between the metal and $NbSe_3$ is conducting. Since CDW properties are extremely sensitive to disorder, these results also indicate that the fabrication process does not in any way disrupt the remaining crystal.

Phase slip is likely to be more sensitive to the details of how current is injected at current contacts than many other CDW phenomena, especially in fully gapped CDW materials. In previous studies of phase slip, current contacts were applied to the side of the crystal and far from its ends. Electric fields applied between side contacts cause depinning, deformations, and transient motion of the CDW 50–100 μm beyond the contacts,[11] offset by a backflow of single particles. Inhomogeneous current and electric field profiles near side-current contacts introduce shear strains in the CDW that may affect plastic failure and drive glide of CDW dislocations away from the contact.[12] The use of side-current contacts may thus affect the details of the phase-slip process in the region where most slip occurs.

In contrast to end contacts, CDW order, deformations, motion, and phase slip abruptly end at the contact, and current is injected purely longitudinally so there is no shear. End contacts should thus give results that can be interpreted with greater confidence, and that can confirm or refute conclusions drawn from side-contact experiments. It could also be expected that submicron size separation of probes will produce qualitatively different phase-slip results.[21]

To characterize how end contacts affect the phase-slip process, I-V measurements were performed in normal (N) and transposed (T) four probe configurations.[6,9,10] In the normal configuration, current is injected through the outer pair of contacts, and the voltage is measured across the inner pair; in the transposed configuration, the roles of the contacts are reversed.

As long as conduction is Ohmic (linear), the voltages V_T and V_N measured in these two configurations for a given current should be the same. However, once the CDW depins, V_T becomes larger than V_N because V_T must not only drive CDW motion in the bulk but also create the deformations near the current contacts that drive the phase slip needed for steady motion. In a simplified model that neglects deformations beyond the current contacts,[7] the voltage difference is related to the phase-slip voltage V_{PS} by

$$V_{PS} = (V_T - V_N)\left(\frac{L_{out}}{L_{out} - L_{in}}\right), \quad (1)$$

where L_{out} and L_{in} denote the length of the sample segment between the inner and outer contact pair, respectively. V_{PS} is roughly proportional to the CDW strain near the current contacts. Assuming homogeneous nucleation of dislocation loops driven by the corresponding CDW stress, V_{PS} can be related to the CDW current—proportional to the total phase-slip rate—by[7]

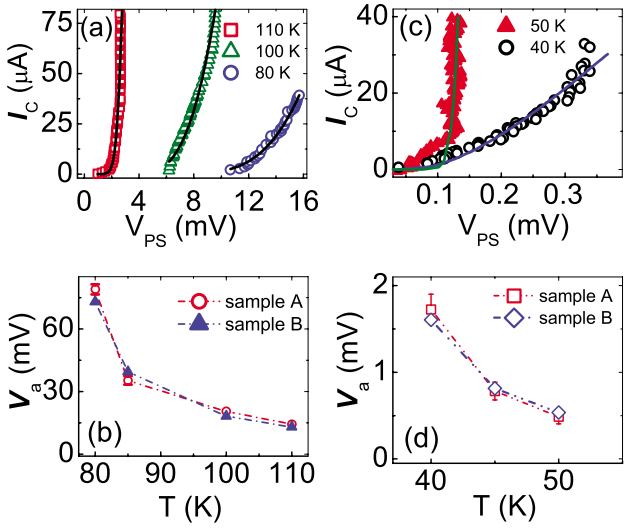

FIG. 4. (Color online) (a) CDW current I_C versus phase-slip voltage V_{PS} at several temperatures, and (b) phase-slip activation voltage V_a versus temperature, for the $T_{P1}=145$ K CDW in $NbSe_3$. [(c) and (d)] Corresponding results for the $T_{P1}=59$ K CDW in $NbSe_3$. Solid lines in (a) and (c) are fits of data from sample A to Eq. (2). Lines in (b) and (d) are guides to the eyes.

$$I_C = I_0 \frac{V_{PS}}{V_a} \exp\left(-\frac{V_a}{V_{PS}}\right). \tag{2}$$

Here, I_0 is related to the attempt rate and V_a is the activation voltage for the phase dislocation loop nucleation. Although the model assumes hard boundary conditions and homogeneous current injection, it gives a good qualitative and semiquantitative account of measurements using side contacts on the $T_{P1}=145$ K CDW in $NbSe_3$.[10] How are measurements affected when hard boundary conditions are imposed using end-current contacts?

Figures 4(a) and 4(b) show results obtained for the T_{P1} CDW in $NbSe_3$. Figure 4(a) shows I_C-V_{PS} measurements at several temperatures. Consistent with results from side contacts, I_C is negligibly small up to a threshold V_{PS}, beyond which I_C increases very rapidly. As shown by the solid lines, the data can be well fitted using Eq. (2). The lower left graph shows how the activation voltage V_a obtained from these fits varies with temperature. The temperature variation and the overall magnitude of V_a are similar (to within the roughly 30% scatter in previous results[10]) to those obtained using side contacts. This similarity may result because only part of the Fermi surface is removed by formation of the T_{P1} CDW. The depinned CDW's conductance is only about 30% of the conductance from the ungapped Fermi surface,[22] and so effects associated with injection from side contacts are less pronounced. The strongly nonlinear dependence of slip rate on phase strain and the interaction between the slip distribution and the strain profile[11,13] may also provide a feedback mechanism that reduces differences V_{PS} for a given I_C and thus V_a in different current injection conditions.

Figures 4(c) and 4(d) show result for the T_{P2} CDW, for temperatures above the "switching" regime. Formation of the $T_{P2}=59$ K CDW removes most of the remaining Fermi surface, and at $T=40$ K the depinned CDW's conductance is roughly 3.3 times that of the single-particle conductance. The single-particle conductance anisotropy is also larger than that of the T_{P1} CDW.[1] As a result, differences between side- and end-current injection should be more apparent. In Fig. 4(c), although I_C increases steeply with V_{PS} at large V_{PS}, it does not show the threshold behavior of the T_{P1} CDW. This issue will be further explored as end contacts are more sensitive probe of the phase loop dynamics. V_a obtained from best fits to the large V_{PS} region increases with decreasing temperature, as for the T_{P1} CDW. The magnitudes of V_{PS} and V_a are roughly a factor of 2 smaller than those reported previously with side contacts,[10] and a factor of 13 smaller at comparable T/T_P than those for the T_{P1} CDW. Thus, the present experiments with end contacts are qualitatively consistent but show some quantitative differences with previous experiments using side contacts only in modestly anisotropic, semimetallic $NbSe_3$.

We have developed a method for fabricating end-current contacts to fibrous, whiskerlike quasi-1D materials. The contacts are robust and give extremely low contact resistances and uniform longitudinal current injection. They should be especially useful for studying more anisotropic and fully gapped materials such as TaS_3, where the poorly understood interplay between the CDW condensate and quasiparticles is more important, and where spreading resistances and inhomogeneous current flow associated with side-current contacts have severely limited interpretation of transport measurements.

End contacts provide a hard boundary condition beyond which there is no CDW order, strain, or motion. They ensure that phase slip occurs in the exposed regions beside the contacts, and not beneath them as is the case with side-current contacts. They can thus be used to probe the CDW strain, structure, and excitation spectrum in the regions of highest slip rate using x-ray microbeam[14] or spatially resolved optical measurements.[15] Such measurements may directly reveal CDW disorder associated with the proliferating dislocations and the midgap soliton excitations which are predicted to form during charge injection and to condense onto dislocation lines, allowing them to climb.[23] The hard boundary condition provided by end contacts should also be ideal for studying CDW physics at scales below 10 μm, allowing well-defined CDW "boxes" to be created and to be probed along the axis of collective excitations and transport. We also expect that the method will also be useful in Hall effect studies and other transport studies.

Microfabrication was performed at the Cornell Nanofabrication Facility (CNF), which is supported by the NSF and the NY-STAR. This work was supported by NSF Grant No. DMR 04-05500. NSLS-BNL is supported by the U.S. DOE, Office of Science, Office of Basic Energy Sciences.

*isakovic@bnl.gov
†Present address: National Institute for Standards and Technology, Boulder, CO.

[1] N. P. Ong and J. W. Brill, Phys. Rev. B **18**, 5265 (1978); E. Slot and H. S. J. van der Zant, J. Phys. IV **12**, Pr9 (2002); K. O'Neill, E. Slot, H. S. J. van der Zant, and R. E. Thorne, *ibid.* **12**, Pr9 (2002).

[2] G. Mihaly, P. Beauchene, T. Chen, L. Mihaly, and G. Gruner, Phys. Rev. B **37**, 6536 (1988).

[3] Yu. I. Latyshev, P. Monceau, A. P. Orlov, S. A. Brazovskii, and Th. Fournier, Supercond. Sci. Technol. **20**, S87 (2007); A. A. Sinchenko, Yu. I. Latyshev, S. G. Zybtsev, I. G. Gorlova, and P. Monceau, Phys. Rev. B **60**, 4624 (1999); E. Canadell, I. E.-I. Rachidi, J. P. Pouget, P. Gressier, A. Meerschaut, J. Rouxel, D. Jung, M. Evain, and M.-H. Whangbo, Inorg. Chem. **29**, 1401 (1990); J. Schafer, M. Sing, R. Claessen, E. Rotenberg, X. J. Zhou, R. E. Thorne, and S. D. Kevan, Phys. Rev. Lett. **91**, 066401 (2003).

[4] E. Slot, H. S. J. van der Zant, and R. E. Thorne, Phys. Rev. B **65**, 033403 (2001).

[5] P. A. Lee and T. M. Rice, Phys. Rev. B **19**, 3970 (1979); L. P. Gorkov, JETP Lett. **38**, 87 (1983); N. P. Ong, G. Verma, and K. Maki, Phys. Rev. Lett. **52**, 663 (1984).

[6] J. C. Gill, J. Phys. C **19**, 6589 (1986).

[7] K. Maki, Physica B & C **143B**, 59 (1986); S. Ramakrishna, M. P. Maher, V. Ambegaokar, and U. Eckern, Phys. Rev. Lett. **68**, 2066 (1992).

[8] D. Feinberg and J. Friedel, in *Low dimensional Electronic Properties of Molybdenum Bronzes and Oxides*, edited by C. Schlenker (Kluwer, Dordrecht, 1989).

[9] D. V. Borodin, S. V. Zaitsev-Zotov, and F. Ya. Nad', Sov. Phys. JETP **66**, 793 (1987); F. Ya. Nad', in *Modern Problems in Condensed Matter Sciences*, edited by L. P. Gor'kov and G. Gruner (North-Holland, Amsterdam, 1989).

[10] M. P. Maher, T. L. Adelman, S. Ramakrishna, J. P. McCarten, D. A. DiCarlo, J. P. McCarten, and R. E. Thorne, Phys. Rev. Lett. **68**, 3084 (1992); Phys. Rev. B **52**, 13850 (1995).

[11] T. L. Adelman, M. C. de Lind van Wijngaarden, S. V. Zaitsev-Zotov, D. DiCarlo, and R. E. Thorne, Phys. Rev. B **53**, 1833 (1996); S. G. Lemay, M. C. de Lind van Wijngaarden, T. L. Adelman, and R. E. Thorne, *ibid.* **57**, 12781 (1998).

[12] J. C. Gill, in *Physics and Chemistry of Low Dimensional Conductors*, NATO Science Series Vol. 354, Proceedings of NATO ASI, Les Houches, 1996, edited by C. Schlenker, J. Dumas, and M. Greenblatt (Plenum, NY, 1996); S. Brazovskii and S. Matveenko, Synth. Met. **56**, 2696 (1993).

[13] S. Brazovskii, N. Kirova, H. Requardt, F. Ya. Nad, P. Monceau, R. Currat, J. E. Lorenzo, G. Grubel, and Ch. Vettier, Phys. Rev. B **61**, 10640 (2000).

[14] D. DiCarlo, E. Sweetland, M. Sutton, J. D. Brock, and R. E. Thorne, Phys. Rev. Lett. **70**, 845 (1993); H. Requardt, F. Ya. Nad, P. Monceau, R. Currat, J. E. Lorenzo, S. Brazovskii, N. Kirova, G. Grubel, and Ch. Vettier, *ibid.* **80**, 5631 (1998).

[15] M. E. Itkis and J. W. Brill, Phys. Rev. Lett. **72**, 2049 (1994); M. E. Itkis, B. M. Emerling, and J. W. Brill, Phys. Rev. B **52**, R11545 (1995); L. Ladino, J. W. Brill, M. Freamat, M. Uddin, and D. Dominko, *ibid.* **74**, 115104 (2006).

[16] H. S. J. van der Zant, A. Kalwij, O. C. Mantel, N. Markovic, Yu. I. Latyshev, B. Pannetier, and P. Monceau, J. Phys. IV **9**, 157 (1999).

[17] F. Y. Nad', M. E. Itkis, P. Monceau, and M. Renard., J. Phys. IV **3**, 175 (1993).

[18] K. Cicak, Ph.D. thesis, Cornell University, 2007.

[19] S. Guan, K. Vollmers, A. Subramanian, and B. J. Nelson, J. Appl. Phys. **97**, 10R506 (2005).

[20] N. Markovic, M. A. H. Dohmen, and H. S. J. van der Zant, Phys. Rev. Lett. **84**, 534 (2000); O. C. Mantel, F. Chalin, C. Dekker, H. S. J. van der Zant, Yu. I. Latyshev, B. Pannetier, and P. Monceau, *ibid.* **84**, 538 (1999); T. Matsuura, T. Tsuneta, K. Inagaki, and S. Tanda, Phys. Rev. B **73**, 165118 (2006); R. Escuedro, A. Briggs, and P. Monceau, J. Phys.: Condens. Matter **13**, 6285 (2001).

[21] H. S. J. Van der Zant, E. Slot, S. V. Zaitsev-Zotov, and S. N. Artemenko, Phys. Rev. Lett. **87**, 126401 (2001).

[22] N. P. Ong, J. W. Brill, J. C. Eckert, J. W. Savage, S. K. Khanna, and R. B. Somoano, Phys. Rev. Lett. **42**, 811 (1979).

[23] S. Brazovskii, in *Physics and Chemistry of Low Dimensional Conductors*, NATO Science Series Vol. 354, Proceedings of NATO ASI, Les Houches, 1996, edited by C. Schlenker, J. Dumas, and M. Greenblatt (Plenum, NY, 1996).